Proceedings of the 4th International Conference on Mechatronics and Smart Systems
DOI: 10.54254/2755-2721/2026.33400

The Effect of Liquid Cooling Flow Rate on the Temperature Field and Temperature Uniformity of Bottom-cooled Plate-type Power Battery Modules

Peike Li

School of Minerals Processing and Bioengineering, CUS University, Changsha, China
lipeike13787268813@163.com

Abstract. We investigated how liquid cooling flow rate influences the temperature field and temperature uniformity of a bottom-cooled plate-type power battery module. Fluent simulation results were compared for six inlet velocities, namely 0.1, 0.2, 0.4, 0.6, 0.8, and 1.0 m/s. The analysis did not rely on a single output image. Instead, the geometry, mesh quality, convergence history, and temperature contours were examined together so that the thermal behavior under each condition could be read in a consistent way. The maximum temperature, minimum temperature, and maximum temperature difference were then extracted from the contour scales and used as the main evaluation indices. The results show a stable vertical thermal gradient in the bottom-cooled configuration. The area close to the cooling plate remains cooler, while the upper part of the module retains a comparatively high temperature. As inlet velocity increases, the hot region in the upper section becomes smaller and the overall temperature level drops. The maximum temperature decreases from 336 K to 330 K, the minimum temperature stays close to 300 K, and the maximum temperature difference is reduced from 36 K to 30 K. The most noticeable improvement appears in the range of 0.1-0.6 m/s. Beyond that point, higher flow rate still helps, but the gain becomes small. In practical terms, flow-rate regulation can improve the thermal response of the module, yet it cannot by itself remove the upper-hot/lower-cool pattern created by bottom cooling. Further improvement in temperature uniformity will still depend on cold-plate design and on shortening the heat-transfer path inside the module.

Keywords: Power battery, Liquid cooling, Cold plate, Temperature field, Temperature uniformity, Numerical simulation

1. Introduction

Battery packs in electric vehicles now operate under higher power demand, faster charging rates, and tighter packaging space than before [1,2]. Under these conditions, heat builds up quickly and places greater pressure on thermal control and safe operation of the pack [1,2]. If local temperature remains much higher in one part of the module than in another, cell aging becomes less uniform and the whole pack is harder to manage in a stable way [1,2]. For that reason, battery thermal

© 2026 The Authors. This is an open access article distributed under the terms of the Creative Commons Attribution License 4.0 (https://creativecommons.org/licenses/by/4.0/).

DOI: 10.54254/2755-2721/2026.33400

management studies usually pay attention to two basic targets at the same time: limiting the peak temperature and improving temperature uniformity [3-5].

Among the available thermal management options, liquid cooling remains attractive because of its comparatively high heat-removal capability and because liquid-based systems can be implemented in several structural forms [6]. Recent studies on liquid-cooled battery modules have largely moved in two directions. One group focuses on structural optimization, such as comparing different liquid-cooling layouts [7,8], redesigning the cooling plate and channel path [9], or examining interface-related effects such as TIM compression ratio [10]. Another group emphasizes system-level modeling and optimization under different operating conditions, including inlet temperature, flow rate, and flow velocity [11,12]. From an engineering point of view, the second route is especially practical in the early design stage, because flow velocity can usually be adjusted more easily than the internal structure of the cooling plate.

The bottom-cooled arrangement considered here has a very specific thermal feature. Heat generated in the upper part of the cell stack does not leave the system directly; it must first travel downward through the battery body before it reaches the cooling plate and the flowing coolant. That path is simple, but it also makes vertical non-uniformity hard to avoid. In low-flow cases, the plate extracts heat slowly and the hottest region remains concentrated in the upper part of the module. When the coolant moves faster, convective heat transfer at the plate side improves and the hot region shrinks. Still, that trend does not continue indefinitely. Once the fluid-side resistance has been lowered to a certain level, the main restriction shifts to conduction through the battery itself and to the fact that cooling is applied only from the bottom. Studying flow rate under this configuration is therefore useful for two reasons: it helps identify the velocity range that actually produces a visible benefit, and it shows where structural modification will still be necessary.

With that issue in mind, we used Fluent simulation results to compare the temperature field of a bottom-cooled plate-type battery module at six inlet velocities. The analysis begins with the model geometry, grid division, and convergence behavior so that the numerical results can be judged on a clear basis. We then read the temperature contours case by case and extracted three temperature indices, namely the maximum temperature, the minimum temperature, and the maximum temperature difference. These indices were used to describe how the module responds as the cooling flow rate increases.

2. Models and methods

2.1. Physical model and grid division

Figure 1 presents the bottom-cooled plate-type battery module considered in this work. In Figure 1(a), the model consists of three square battery cells, a cooling plate positioned beneath the cells, and the corresponding coolant inlet and outlet. Coolant enters through the inlet, flows through the internal passages of the plate, and leaves through the outlet, while the heat generated in the cells is conducted downward and removed by the plate. Small local features that do not affect the main heat-transfer route were simplified so that the model stayed focused on the dominant thermal process.

The mesh used for the coupled analysis is shown in Figure 1(b). An unstructured grid was adopted for the whole domain, and local refinement was added near the battery-cooling-plate contact surfaces, the internal flow passages, and the inlet and outlet regions. This treatment makes the solid-fluid interface easier to resolve and improves the description of local flow development in the

DOI: 10.54254/2755-2721/2026.33400

channel. The final mesh remains fairly even in the rest of the domain, which is adequate for the present conjugate heat-transfer simulation.

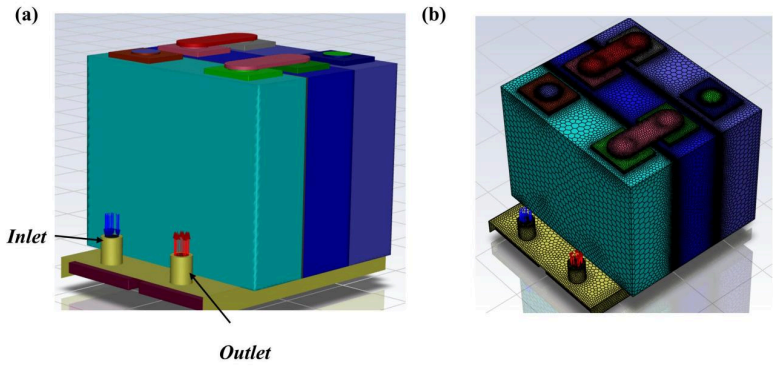


Figure 1. Geometric model and meshing results of liquid-cooled battery module: (a) Geometric model; (b) Meshing results

2.2. Basic assumptions

To keep the comparison centered on inlet velocity, several simplifying assumptions were introduced. The coolant was treated as an incompressible steady flow, and heat generation inside each battery cell was assumed to be uniform. Material properties were taken as constants over the calculation range, thermal radiation was neglected, and only solid conduction together with fluid convection was considered. In addition, the thermal contact between the battery and the cooling plate was assumed to be good enough that no extra contact resistance had to be introduced in the model. These assumptions are conventional for this type of numerical study and help keep the comparison between the six operating conditions straightforward.

2.3. Operating conditions and data extraction methods

Six inlet velocities were considered in the simulation, namely 0.1, 0.2, 0.4, 0.6, 0.8, and 1.0 m/s. For each case, the available post-processing information includes the model geometry, the grid, the convergence curves, and the temperature contours. To compare the six cases on the same basis, we read the upper and lower limits of the contour scale as the maximum and minimum temperatures, respectively, and then calculated the maximum temperature difference using Equation (1). This reading method is simple, but it is well suited to the material currently available from the Fluent post-processing results.

$$\Delta T = T_{\max} - T_{\min} \tag{1}$$

Because the contour scale is displayed with limited precision, the extracted temperatures were retained as integer Kelvin values and were converted to °C only when the discussion required a direct engineering interpretation. The temperature data from the six cases were then arranged into a single set and used to plot the characteristic temperature curves and the maximum temperature difference curve. In this way, the visual information in the contours could be linked to quantitative trends without introducing additional processing steps that were not supported by the existing output files.

DOI: 10.54254/2755-2721/2026.33400

3. Results and analysis

3.1. Analysis of numerical convergence characteristics

Figure 2 gives the convergence history for a representative operating condition. In Figure 2(a), the volume-average temperature rises quickly during the initial iterations and then settles gradually after roughly 60-80 iterations, which suggests that the coupled solution of flow and heat transfer is approaching a stable state. Figure 2(b) shows the residual history of the governing equations. The continuity, momentum, and energy residuals all decrease as the iteration proceeds, and the energy residual shows the clearest downward trend. This is what one would expect once the temperature field begins to settle.

The residuals do not fall at exactly the same rate, but they remain well behaved throughout the solution process and no obvious divergence is observed. Read together, Figure 2(a) and Figure 2(b) support the reliability of the numerical results used in the later sections. That matters here because the discussion that follows depends on relatively small temperature changes between some of the higher-velocity cases.

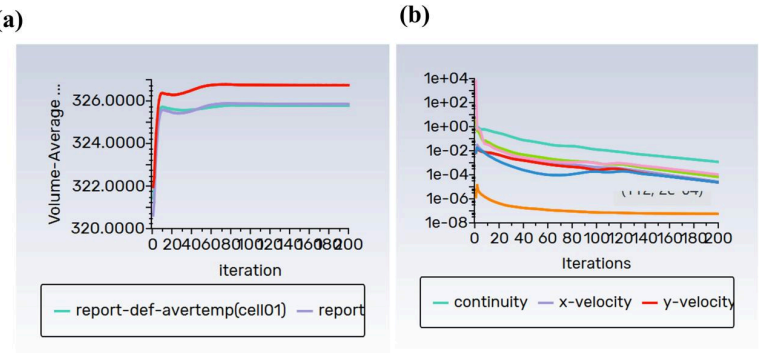


Figure 2. Convergence process of numerical computation: (a) Monitoring curve of bulk average temperature; (b) Residual convergence curve

3.2. Temperature field distribution characteristics at different liquid cooling flow rates

Figure 3 shows the temperature contours at the six inlet velocities. A common pattern appears in every case. The region close to the bottom cooling plate stays cooler, while the temperature rises gradually toward the upper part of the battery. In other words, the temperature field is governed mainly by a vertical gradient rather than by a strong left-right imbalance. This distribution fits the physical layout of the module: heat must travel from the battery body to the lower cooling surface before it can be removed by the coolant.

At 0.1 m/s, the stratification visible in Figure 3 is the most pronounced. A relatively broad cool region is confined to the area close to the plate, but the upper part of the module still forms a clear hot zone. This makes the limitation of low-flow operation easy to see. When the inlet velocity is raised to 0.2 and then 0.4 m/s, the cool region extends upward and the hot area contracts. The change is not only visible in size; the overall contour distribution also becomes less severe than in the lowest-flow case.

The trend continues at 0.6, 0.8, and 1.0 m/s, but the magnitude of the change becomes much smaller. The lower portion of the module hardly changes at these higher velocities, and the hot region in the upper part weakens only slightly. That behavior is useful because it points to the real bottleneck of the present structure. Once the flow at the plate side is already strong enough, further

DOI: 10.54254/2755-2721/2026.33400

increase in coolant velocity cannot substantially shorten the path through which heat must move inside the battery before reaching the cold plate. For this reason, Figure 3 is less a story of continuous improvement than a story of diminishing returns. The main thermal problem remains the persistent upper-hot/lower-cool pattern, not a strong lateral temperature offset.

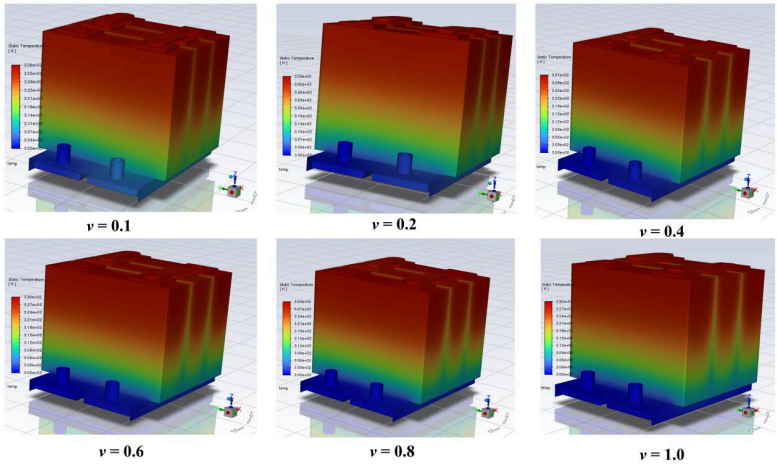


Figure 3. Temperature cloud map of modules under different liquid cooling flow rates. From left to right and top to bottom, the flow rates are v=0.1, 0.2, 0.4, 0.6, 0.8, and 1.0 m/s

3.3. Effect of liquid cooling flow rate on characteristic temperature parameters

The characteristic temperatures extracted from the contour scales in Figure 3 are summarized in Table 1, which provides a more direct numerical comparison among the six operating conditions.

Table 1. Characteristic temperature parameters under different liquid cooling flow rate conditions

Operating condition code	Inlet flow rate /m·s^{-1}	Max temperature K	Min temperature K	Difference K
Case 1	0.1	336	300	36
Case 2	0.2	333	300	33
Case 3	0.4	331	300	31
Case 4	0.6	330	300	30
Case 5	0.8	330	300	30
Case 6	1.0	330	300	30

Figure 4 plots the maximum and minimum temperatures as functions of inlet velocity. As the velocity increases from 0.1 to 1.0 m/s, the maximum temperature falls from 336 K to 330 K, which corresponds to a decrease from 62.85 °C to 56.85 °C. By contrast, the minimum temperature remains close to 300 K, or about 26.85 °C, throughout the whole range. This difference between the two curves is meaningful. It suggests that increasing flow rate mainly cools the hotter part of the module, while the coolest region is already constrained by its proximity to the cooling plate and to the coolant inlet. Put simply, the colder region has little room to drop further, whereas the upper hot region still responds to additional cooling.

The drop in maximum temperature is concentrated in the low-to-moderate velocity range. When the inlet velocity rises from 0.1 to 0.2 m/s, the maximum temperature decreases by 3 K. Raising the velocity again to 0.4 m/s produces another 2 K reduction. After that, the curve becomes much flatter.

DOI: 10.54254/2755-2721/2026.33400

Once the velocity exceeds 0.6 m/s, the remaining decrease is only about 1 K and then nearly disappears. For engineering design, this point is important because it marks the range in which pumping more coolant begins to bring less obvious thermal benefit under the present module structure.

Figure 5 shows that the maximum temperature difference follows a similar pattern. It falls from 36 K at 0.1 m/s to 30 K at 1.0 m/s, and most of that reduction occurs before the inlet velocity reaches 0.6 m/s. After that, the curve approaches a plateau. Part of the reason is physical: stronger fluid-side heat transfer cannot fully overcome the vertical conduction resistance between the upper battery region and the bottom plate. Part of the reason also comes from the way the data were read. Because the contour scales were interpreted at integer-Kelvin precision, differences smaller than 1 K among the cases of 0.6, 0.8, and 1.0 m/s appear as the same value in the present comparison.

When Figure 4 and Figure 5 are considered together, a consistent picture emerges. Increasing flow rate does improve the thermal behavior of the bottom-cooled module, especially by suppressing the hottest region, but the improvement is bounded by the structure itself. Even at 1.0 m/s, the module still shows a temperature difference of about 30 K, which means that the upper-hot/lower-cool stratification remains evident. In practice, then, velocity regulation should be regarded as one useful control parameter rather than a complete solution. If a more uniform temperature field is required, the design will also need better cooling coverage, a revised cold-plate structure, or a shorter internal heat-transfer path.

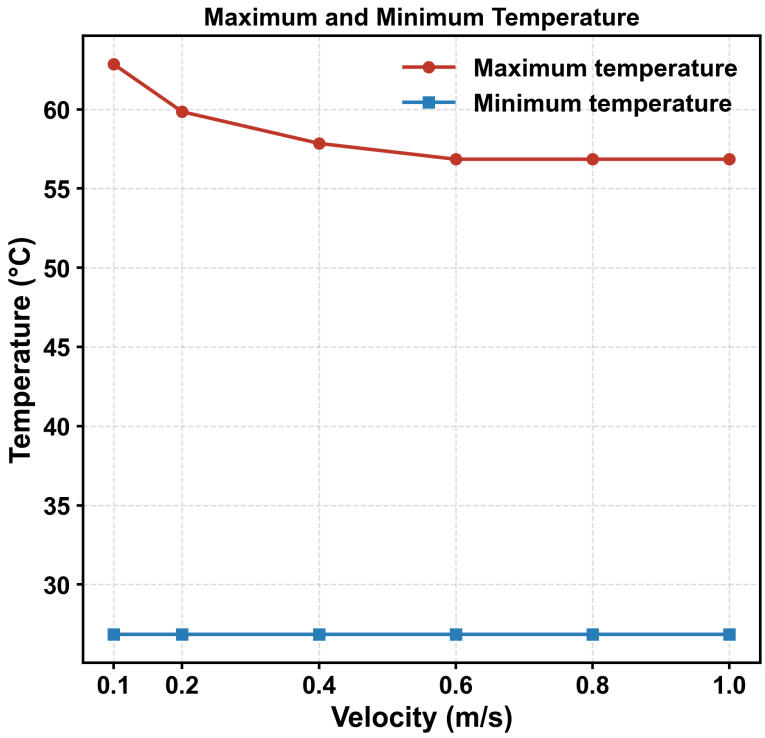


Figure 4. Maximum and minimum temperatures versus liquid cooling flow rate

DOI: 10.54254/2755-2721/2026.33400

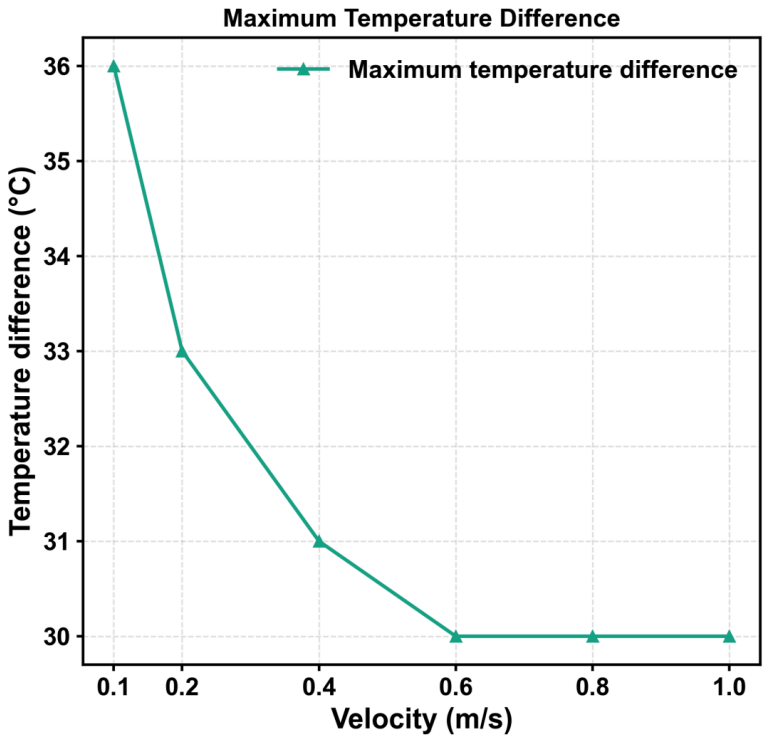


Figure 5. Maximum temperature difference versus liquid cooling flow rate

4. Conclusion

This study examined the temperature field of a bottom-cooled liquid-cooled battery module at six inlet velocities by using Fluent simulation results. Across all operating conditions, the module maintained a clear vertical temperature gradient: the region near the cooling plate stayed cooler, while the upper part of the module remained hotter. As the inlet velocity increased from 0.1 to 1.0 m/s, the maximum temperature decreased from 336 K to 330 K, the minimum temperature stayed close to 300 K, and the maximum temperature difference was reduced from 36 K to 30 K. These results show that increasing flow rate is effective, but mainly in the sense of easing the hot spot rather than fully equalizing the whole module.

The strongest improvement appeared in the range of 0.1-0.6 m/s. Beyond that interval, the temperature curves changed only slightly, which suggests that the controlling resistance gradually shifted away from the fluid side and toward the conduction path inside the battery together with the bottom-only cooling layout. In other words, higher flow rate helps, but it does not remove the basic structural reason for the upper-hot/lower-cool distribution. Future optimization of this type of module should therefore combine flow regulation with structural measures such as redesigning the cold plate, enlarging effective cooling coverage, or improving the internal heat-transfer route.

References

[1] He L, Gu Z, Zhang Y, et al. Review on thermal management of lithium-ion batteries for electric vehicles: advances, challenges, and outlook [J]. Energy & fuels, 2023, 37(7): 4835-4857.

[2] Rahmani A, Dibaj M, Akrami M. Recent advancements in battery thermal management systems for enhanced performance of Li-ion batteries: A comprehensive review [J]. Batteries, 2024, 10(8): 265.

[3] Zhou R, Chen Y, Zhang J, et al. Research progress in liquid cooling technologies to enhance the thermal management of LIBs [J]. Materials Advances, 2023, 4(18): 4011-4040.

DOI: 10.54254/2755-2721/2026.33400

[4] Zhao G, Wang X, Negnevitsky M, et al. An up-to-date review on the design improvement and optimization of the liquid-cooling battery thermal management system for electric vehicles [J]. Applied Thermal Engineering, 2023, 219: 119626.
[5] Anisha, Kumar A. Identification and mitigation of shortcomings in direct and indirect liquid cooling-based battery thermal management system [J]. Energies, 2023, 16(9): 3857.
[6] Xu J, Guo Z, Xu Z, et al. A systematic review and comparison of liquid-based cooling system for lithium-ion batteries [J]. ETransportation, 2023, 17: 100242.
[7] Murphy M, Akrami M. Advanced thermal management of cylindrical lithium-ion battery packs in electric vehicles: a comparative CFD study of vertical, horizontal, and optimised liquid cooling designs [J]. Batteries, 2024, 10(8): 264.
[8] Angani A, Kim H W, Hwang M H, et al. A comparison between Zig-Zag plated hybrid parallel pipe and liquid cooling battery thermal management systems for Lithium-ion battery module [J]. Applied Thermal Engineering, 2023, 219: 119599.
[9] Wang Z, Wang X, Liang G, et al. Topology optimization design and thermofluid performance analysis of li-ion battery cooling plate [J]. Structural and Multidisciplinary Optimization, 2024, 67(11): 198.
[10] Gu J, Kim H K, Jang S. Study of cooling performance of liquid-cooled ev battery module according to the Tim compression ratio [J]. International Journal of Automotive Technology, 2025, 26(2): 359-373.
[11] Chen Y, Hu Z. Computational fluid dynamic modeling of pack-level battery thermal management systems in electric vehicles [J]. Energies, 2025, 18(3): 484.
[12] Niu Z, Pang K, Pang B, et al. Orthogonal experimental-based thermal management design and simulation optimization of a liquid-cooled battery module [J]. Scientific Reports, 2025, 15(1): 33442.